

The role of strain hardening in the transition from dislocation-mediated to frictional deformation of marbles within the Karakoram Fault Zone, NW India

David Wallis^{a,c,*}, Geoffrey E. Lloyd^b, Lars N. Hansen^a

^a Department of Earth Sciences, University of Oxford, Oxford, OX1 3AN, UK

^b School of Earth and Environment, University of Leeds, Leeds, LS2 9JT, UK

^c Department of Earth Sciences, Utrecht University, Utrecht, 3584 CD, Netherlands

ARTICLE INFO

Keywords:

Calcite
Schmid factor
Resolved shear stress
Strain hardening
Seismogenesis
Karakoram Fault Zone

ABSTRACT

The onset of frictional failure and potentially seismogenic deformation in carbonate rocks undergoing exhumation within fault zones depends on hardening processes that reduce the efficiency of aseismic dislocation-mediated deformation as temperature decreases. However, few techniques are available for quantitative analysis of dislocation slip system activity and hardening in natural tectonites. Electron backscatter diffraction maps of crystal orientations offer one such approach via determination of Schmid factors, if the palaeostress conditions can be inferred and the critical resolved shear stresses of slip systems are constrained. We analyse calcite marbles deformed in simple shear within the Karakoram Fault Zone, NW India, to quantify changes in slip system activity as the rocks cooled during exhumation. Microstructural evidence demonstrates that between ~300 °C and 200–250 °C the dominant deformation mechanisms transitioned from dislocation-mediated flow to twinning and frictional failure. However, Schmid factor analysis, considering critical resolved shear stresses for yield of undeformed single crystals, indicates that the fraction of grains with sufficient resolved shear stress for glide apparently increased with decreasing temperature. Misorientation analysis and previous experimental data indicate that strain-dependent work hardening is responsible for this apparent inconsistency and promoted the transition from dislocation-mediated flow to frictional, and potentially seismogenic, deformation.

1. Introduction

Calcite exhibits marked velocity-weakening behaviour, which may promote nucleation of unstable earthquake ruptures (Han et al., 2010; Verberne et al., 2015; Cowie et al., 2017). Faults hosted in calcite-rich lithologies are therefore major sources of seismic hazard in zones of active continental deformation (Smith et al., 2011). The depth extent of earthquake nucleation in such faults broadly corresponds to the depth at which the activity of temperature-dependent aseismic creep processes can prevent unstable frictional failure under interseismic strain rate conditions (Scholz, 1988; Verberne et al., 2015). Dislocation-mediated deformation mechanisms (potentially including contributions from dislocation creep, low-temperature plasticity, and/or dislocation-accommodated grain boundary sliding) are commonly inferred to have operated in calcite-rich shear zones exhumed from mid-crustal depths and in which the grain size and/or conditions were unfavourable for efficient diffusion creep (e.g. Bestmann et al., 2006; Rutter et al., 2007; Wallis et al., 2013; Parsons et al., 2016). Therefore, competition

between dislocation-mediated flow and frictional failure may exert an important control on the depth limit of earthquake nucleation. However, the precise microphysical processes that control this transition in natural fault zones remain poorly constrained, particularly in situations where rocks are progressively exhumed during deformation, resulting in a transition from aseismic flow to potentially seismogenic frictional failure within the exhuming rock mass (Handy et al., 2007). The strength of rocks undergoing dislocation-mediated deformation is a function of the stresses required to activate dislocation glide on particular crystallographic slip systems, which may depend on both environmental conditions (e.g. temperature, pressure, and strain rate) and other state variables (e.g. composition, dislocation density and distribution) (e.g., Hobbs et al., 1972; De Bresser and Spiers, 1997). However, it is challenging to determine the strength and activity of slip systems during dislocation-mediated deformation in natural tectonites, and relatively few techniques are available to do so. As a result, the precise controls on the transition from aseismic creep to frictional failure and potentially seismogenic behaviour in natural fault zones

* Corresponding author. Department of Earth Sciences, University of Oxford, Oxford, OX1 3AN, UK.
E-mail address: David.Wallis@earth.ox.ac.uk (D. Wallis).

remain poorly constrained.

The most common approach to assess the relative activity of different slip systems in natural tectonites is to interpret the slip system(s) most likely to have generated an observed crystallographic preferred orientation (CPO); for example, by determining the slip system inferred to have most readily rotated into orientations with high resolved shear stress (e.g., Toy et al., 2008). However, such analysis is often limited to qualitative interpretations and comparisons. More quantitative information can be gleaned by comparing natural and experimental CPOs to results from simulations of polycrystal plasticity (e.g. Wenk et al., 1987). However, this approach tends to place relatively loose constraints on slip system activity due to the large parameter space that needs to be searched (i.e., typically many combinations of slip system strengths and deformation geometries have to be tested) and challenges in comparing natural and simulated CPO geometries quantitatively.

Another approach is to analyse crystallographic misorientations resulting from the presence of dislocations within grains (Lloyd et al., 1997; Bestmann and Prior, 2003; Wheeler et al., 2009). However, due to the limited angular resolution of commonly available measurement techniques (e.g. $\sim 0.2^\circ$ for misorientation angles from conventional electron backscatter diffraction, EBSD) such analysis can only sample the fraction of the dislocation population that is arranged into relatively high misorientation substructures such as subgrain boundaries (Prior, 1999). As such, ‘free’ dislocations that are not in subgrain boundaries can be difficult to detect and generally require higher precision and more computationally expensive techniques such as high-angular resolution electron backscatter diffraction (Wallis et al., 2016a, 2017). Moreover, it is unclear to what extent the measured dislocation content was glissile or sessile during deformation. This ambiguity also often applies to direct observation of dislocations, by transmission-electron imaging, chemical etching, or decoration by oxidation.

In this contribution, we exploit advances in EBSD (Prior et al., 1999, 2009; Bachmann et al., 2010; Mainprice et al., 2011) to develop a method of slip system analysis based on determination of Schmid factors (Schmid, 1928; Schmid and Boas, 1950; Farla et al., 2011; Hansen et al., 2011). The Schmid factor of a slip system quantitatively describes the relation between resolved shear stress and applied stress state (the higher the Schmid factor, the greater the resolved shear stress on the slip system). This orientation relationship is typically qualitatively inferred when interpreting slip systems that contribute to CPO development (e.g. Toy et al., 2008). However, the Schmid factor not only quantifies this relationship, but also allows for calculation of resolved shear stresses on each slip system, and enables mapping of grains that are (un)favourably oriented for dislocation glide. Relatively few geological studies have utilised detailed Schmid factor analysis. Most of these focussed on stress states associated with radially-symmetric shortening or extension (e.g. Ralser et al., 1991; Farla et al., 2011; Hansen et al., 2011), and to our knowledge, only two have considered simple shear, both focussed on quartz (Law et al., 1990; Toy et al., 2008).

To explore the capabilities of this approach, we conduct a detailed Schmid factor analysis of calcite in marbles deformed within a shear zone of the Karakoram Fault Zone (KFZ), NW India (Fig. 1). Calcite is particularly well suited for Schmid factor analysis because: (1) techniques are well established to infer palaeostress magnitudes and orientations (Turner, 1953; Rowe and Rutter, 1990) as well as metamorphic and deformation temperatures (Covey-Crump and Rutter, 1989; Burkhard, 1993) from calcite microstructures; (2) the critical resolved shear stresses (CRSSs) of calcite slip systems are experimentally constrained (De Bresser and Spiers, 1997); and (3) these CRSSs and the post-yield behaviour exhibit low strain rate sensitivity (stress exponents in the ranges 5.3–42.6 and 9.3–15.5, respectively) indicating near plastic (as opposed to strain rate-sensitive viscous) behaviour when deformed at differential stresses greater than approximately 30 MPa (Wang et al., 1996; De Bresser and Spiers, 1997). The marbles that we investigate have undergone a protracted deformation history

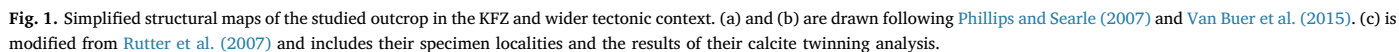
during exhumation and cooling from upper amphibolite-grade conditions to near surface depths and occur in a fault zone that exhibits geomorphological evidence for M_w 7+ earthquakes during the Quaternary (Brown et al., 2002; Rutter et al., 2007; Wallis et al., 2013). We investigate the latter part of this history as the rocks were exhumed and cooled through the frictional-viscous transition zone (Wallis et al., 2013, 2015) and underwent a transition from aseismic flow to potentially seismogenic frictional failure (Rutter et al., 2007). In particular, we use Schmid factor analysis combined with other microstructural observations to test: (1) the manner in which slip system activity potentially varied under evolving temperature and stress conditions during exhumation, (2) the impact of strain hardening on slip system activity, and (3) how these factors affected the transition from crystal plastic to frictional and potentially seismogenic styles of deformation.

2. Geological setting

The KFZ is a > 800 km long fault zone that strikes NW-SE and delineates the western margin of the Tibetan plateau, accommodating dextral displacement resulting from the India-Asia collision (Fig. 1). Along the central KFZ in NW India structures formed at and below lower amphibolite grade are unequivocally attributable to deformation within the KFZ, and record a sequence of fault rocks formed at progressively lower temperature due to ongoing deformation during exhumation (Phillips and Searle, 2007; Wallis et al., 2013, 2015). We investigate marbles deformed within the Pangong strand of the KFZ, adjacent to the Pangong Transpressional Zone (PTZ) (Fig. 1).

Between Muglib and Pangong Tso, the Pangong strand deforms rocks of the Pangong Metamorphic Complex (PMC) and juxtaposes them with the PTZ (Fig. 1). The PMC consists of banded marbles, amphibolites, and pelites that underwent regional metamorphism under kyanite grade (up to $736 \pm 47^\circ\text{C}$ and $1059 \pm 219\text{ MPa}$, Wallis et al., 2014) and sillimanite grade conditions (Streule et al., 2009), followed by retrograde metamorphism and KFZ deformation under lower amphibolite to sub-greenschist conditions (Rutter et al., 2007; Streule et al., 2009; Wallis et al., 2014; Van Buer et al., 2015).

Rutter et al. (2007) studied in detail an outcrop of deformed marble near Muglib ($N34^\circ00'55''$ $E078^\circ17'03''$), providing the context for this study (Fig. 1). Here we summarise the most relevant findings of their study. Grain-shape foliation at this locality dips moderately SW and mineral stretching lineations plunge gently both NW and SE, consistent with the wider KFZ kinematics. Rutter et al. (2007) investigated seven marble samples exhibiting microstructures that record mylonitic fabrics evident as varying degrees of dynamic recrystallisation. From the reconstructed grain size of weakly recrystallised host grains, they estimated metamorphic temperatures in the range $300 \pm 20^\circ\text{C}$ to $480 + 130/-30^\circ\text{C}$, using the grain size-temperature relationship of Covey-Crump and Rutter (1989). These data place an upper limit on the temperature of overprinting deformation in each sample. The grain size of dynamically recrystallised neoblasts indicates flow stresses in the range of $40 \pm 20\text{ MPa}$ to $110 \pm 40\text{ MPa}$ according to the calibration of Rutter (1995) based on dynamic recrystallisation by grain boundary migration. The choice of this calibration, rather than an alternative based on dynamic recrystallisation by subgrain rotation (Rutter, 1995), is supported by our microstructural analysis in the following sections, which reveals irregular grain boundary morphologies but limited subgrain development, consistent with microstructures reported by Rutter et al. (2007). Twin incidence (the percentage of grains, in a given grain size class interval, that contain optically visible twin lamellae) indicates differential stresses in the range of $160 \pm 30\text{ MPa}$ to $250 \pm 30\text{ MPa}$ according to the calibration of Rowe and Rutter (1990). Thick twins exhibit straight, or curved and tapered boundaries indicating temperatures of $200\text{--}250^\circ\text{C}$ (Burkhard, 1993). These constraints, along with observations that the mylonitic fabric is cross-cut by calcite veins that are twinned but not mylonitised, suggest that twinning postdates dynamic recrystallisation (Rutter et al., 2007). Dynamic analysis of



Quaternary deformation on the Pangong strand is recorded by offset debris flows and alluvial fans, which indicate an average slip rate of

For this study we focus on mylonitic marble sample EM1 of [Rutter et al. \(2007\)](#), for which the deformation conditions are particularly well constrained ([Table 1](#), [Fig. 2](#)). Notably, this is one of the lowest temperature samples studied by [Rutter et al. \(2007\)](#), with the size of host grains placing an upper limit of 310 ± 20 °C on the temperature of formation of the mylonitic fabric ([Table 2](#)). This temperature is similar to the temperature of ~ 300 °C estimated for formation of the gouge layer. Therefore, EM1 records mylonitic deformation shortly preceding, or broadly coincident with, the onset of frictional deformation at this structural level. The results derived from detailed analysis of this sample are interpreted in the well-constrained context, outlined above, of evolving deformation processes and conditions as the marbles and surrounding units were exhumed.

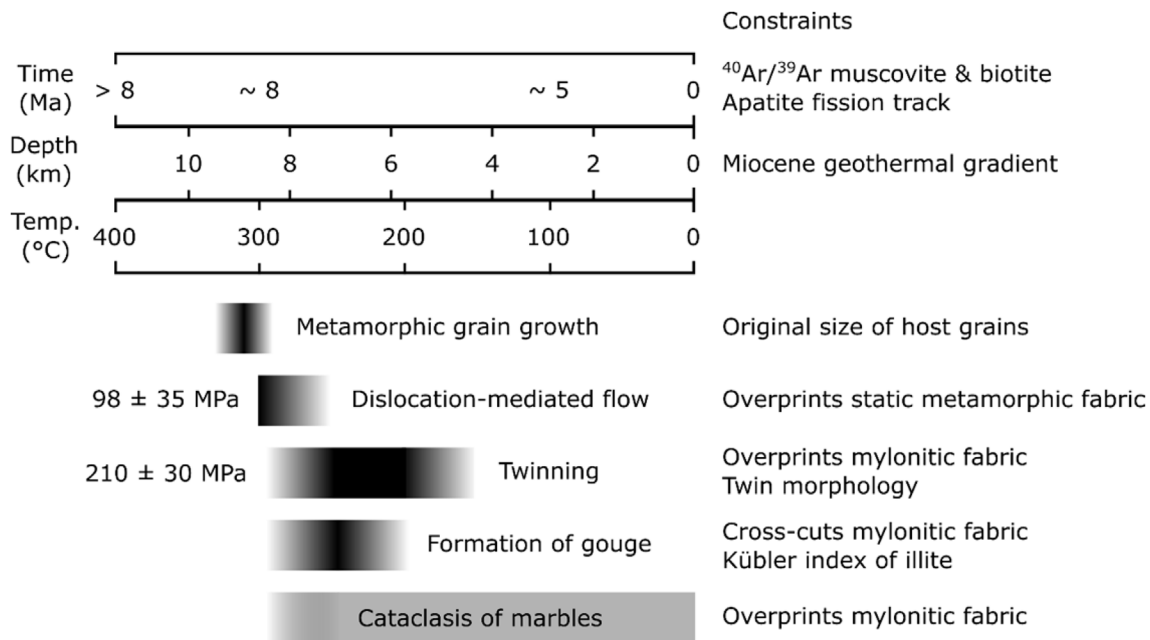


Fig. 2. Summary of constraints on the deformation and exhumation histories of the investigated marble sample EM1 (metamorphic grain growth, dislocation-mediated flow, and twinning) and the surrounding rocks (formation of gouge and cataclasis). Constraints on temperatures of deformation and metamorphic processes, along with differential stresses, are obtained or inferred from Rutter et al. (2007). The Miocene geothermal gradient within the Pangong Transpressional Zone was estimated by Wallis et al. (2014) to be ~ 35 °C/km based on geothermobarometry of migmatites formed at ~ 17 Ma. Time constraints are derived from $^{40}\text{Ar}/^{39}\text{Ar}$ and apatite fission track thermochronology (Boutounet et al., 2012; Wallis et al., 2016b).

3. Methods

A section of sample EM1 of Rutter et al. (2007) was cut parallel to the lineation and perpendicular to the foliation. This section was polished with successively decreasing grit sizes down to 0.25 μm diamond grit, followed by 0.03 μm colloidal silica. Electron backscatter diffraction (EBSD) data were collected on a band of fine-grained matrix calcite using an FEI Quanta 650 FEG E-SEM in the Department of Earth Sciences, University of Oxford. The system is equipped with an Oxford Instruments NordlysNano EBSD camera and AZtec/Channel5 software. Data were collected by automated mapping and consist of 1003×692 points with a step size of 1 μm . 96.9% of the map area was indexed as calcite, and the majority of points that were not indexed were due to the presence of other phases with rare occurrence, such as quartz. The data were processed to remove individual mis-indexed pixels that had $> 10^\circ$ misorientation from all their neighbours. Next, non-indexed pixels with ≥ 7 neighbours belonging to the same grain were filled with the average orientation of their neighbours. Maps of crystal orientation and local misorientation within a 3×3 pixel kernel were produced using Channel5. Pole figures and Schmid factor analyses were computed and plotted using the MATLAB® toolbox MTEX 4.5 (Bachmann et al., 2010; Mainprice et al., 2011). Analysis in MTEX utilised the built-in Schmid-Factor function to operate on *slipSystem* and stress tensor MTEX objects (Supplementary Material). These objects were specified as the relevant

slip systems for calcite and stress tensor for the natural deformation as described below.

The Schmid factor of a slip/twin system describes the fraction of the applied stress that is resolved onto a particular slip/twin plane in the slip/twin direction, and can be described either as a scalar value (Schmid, 1928; Schmid and Boas, 1950) or as a second rank tensor (e.g. Pokharel et al., 2014). In the conventional definition, originally formulated for uniaxial tension (Schmid, 1928; Schmid and Boas, 1950), the Schmid factor (m^s) of a slip/twin system (s) is computed as

$$m^s = \cos \phi \cos \lambda, \quad (1)$$

where ϕ and λ are the angles between the maximum principal stress direction and the slip/twin plane normal and slip/twin direction, respectively. This scalar Schmid factor then relates the applied differential stress (σ_{diff} , i.e., the difference between the maximum and minimum principal stresses) to the shear stress resolved on the slip/twin system (τ^s) by

$$\tau^s = m^s \sigma_{\text{diff}}. \quad (2)$$

The maximum fraction of the differential stress (σ_{diff}) that can be resolved onto a slip/twin plane in the slip/twin direction is 0.5. This corresponds to the maximum value of m^s .

An alternative approach, which allows analysis of varied stress states, is to employ the Schmid tensor. The symmetric Schmid tensor

Table 1
Microstructural data from calcite in EM1 and inferred deformation conditions experienced by sample EM1, from Rutter et al. (2007).

Parameter	Value	Notes
Host grain size (μm)	240 ± 11	Measured from weakly recrystallised grains where the original grain outline could be established.
Dynamically recrystallised grain size (μm)	40 ± 9	Measured from digital maps of several hundred grains following Rutter (1995).
Overall (host and recrystallised) grain size (μm)	48 ± 10	Measured from digital maps of several hundred grains following Rutter (1995).
Temperature (°C)	310 ± 20	From grain size-temperature relationship of marbles on Naxos, Greece, based on Covey-Crump and Rutter (1989). Taken as an approximate upper-bound for the deformation temperature.
Flow stress (differential) (MPa)	98 ± 35	From dynamically recrystallised grain size using the calibration of Rutter (1995).
Twinning stress (differential) (MPa)	210 ± 30	From the twinning incidence piezometric relationship of Rowe and Rutter (1990).

Table 2
Summary of slip system information for EM1.

Deformation temperature (°C)	Slip system	τ_c (MPa)	Applied differential stress (MPa)	Minimum m for twinning/dislocation glide
300	{e}-twinning $\{\bar{1}018\}\langle 40\bar{4}1\rangle$	2	98 ± 35	0.02
300	{r}-slip $\{10\bar{1}4\}\langle 2021\rangle$	22	98 ± 35	0.22
300	{f}-slip $\{\bar{1}012\}\langle 2\bar{2}01\rangle$	52	98 ± 35	0.53
200	{e}-twinning $\{\bar{1}018\}\langle 40\bar{4}1\rangle$	3	210 ± 30	0.01
200	{r}-slip $\{10\bar{1}4\}\langle 2021\rangle$	41	210 ± 30	0.20
200	{f}-slip $\{\bar{1}012\}\langle 2\bar{2}01\rangle$	77	210 ± 30	0.37

(\mathbf{m}^s) describes the projection of the deviatoric stress tensor ($\boldsymbol{\sigma}$, i.e., with the mean stress subtracted from each normal stress) onto a slip/twin system (s), defined by unit vectors describing a slip/twin direction (\mathbf{b}^s) and slip/twin plane normal (\mathbf{n}^s), by

$$\tau^s = \frac{1}{2}(\mathbf{b}^s \otimes \mathbf{n}^s + \mathbf{n}^s \otimes \mathbf{b}^s) : \boldsymbol{\sigma} = \mathbf{m}^s : \boldsymbol{\sigma}, \quad (3)$$

which yields the shear stress resolved on that slip system (τ^s) (for a recent review, see Pokharel et al., 2014). In other words, the components of \mathbf{m}^s determine the fraction of each component in the deviatoric stress tensor that is resolved onto the slip/twin plane in the slip/twin direction. In plastically deforming crystals, dislocation glide or twinning can only occur when τ^s exceeds a threshold value, that is, the critical resolved shear stress (τ_c^s) (Schmid, 1928; Schmid and Boas, 1950). The value of τ_c varies with slip/twinning system, material, and environmental conditions, primarily temperature (e.g. De Bresser and Spiers, 1997; Morales et al., 2014).

To calculate Schmid factors for past deformations, constraints on the palaeo-stress state are required. Differential stresses applied to sample EM1 have been estimated from palaeopiezometric analyses (Table 1; Rutter et al., 2007), but the shape of the stress tensor also needs to be determined. Based on the macroscopic kinematics of the Pangong strand, along with asymmetric deformation microstructures and distributions of foliations, lineations, and palaeostress orientations reported by Rutter et al. (2007) (Fig. 1), we infer that the deformation history of EM1 was dominated by simple shear. To further test the hypothesis that deformation was dominantly simple shear, we apply the approach of Michels et al. (2015) to determine the macroscopic vorticity axis from crystallographic orientation data. This method uses principal geodesic analysis of intragranular orientation dispersion to fit a single ‘crystallographic vorticity axis’ (CVA) to each grain. For samples in which dislocation activity accommodated significant strain, CVAs averaged over many grains may record the vorticity axis of deformation.

Values of the scalar Schmid factor, m^s , can be computed by entering a normalised stress tensor, $\hat{\boldsymbol{\sigma}}$, in the right hand side of Equation (3) to give

$$m^s = \mathbf{m}^s : \hat{\boldsymbol{\sigma}}. \quad (4)$$

Assuming macroscopic simple shear deformation within the Pangong strand, and defining $\hat{\boldsymbol{\sigma}}$ as

$$\hat{\boldsymbol{\sigma}} = \boldsymbol{\sigma} / \sigma_{\text{diff}}, \quad (5)$$

gives

$$\hat{\boldsymbol{\sigma}} = \begin{bmatrix} 0 & 1/2 & 0 \\ 1/2 & 0 & 0 \\ 0 & 0 & 0 \end{bmatrix}. \quad (6)$$

This formulation denotes that the maximum possible value of the shear stress components is half the magnitude of the applied differential stress. This approach is equivalent to that of Law et al. (1990), except that they normalised the shear stress components by their maximum possible magnitude, which leads to non-zero terms in $\hat{\boldsymbol{\sigma}}$ having a value of one and m with values in the range 0–1. In contrast, by normalising the shear stress components by the magnitude of the differential stress,

we obtain values of m in the conventional range 0–0.5, which can be used more directly in conjunction with differential stress magnitudes from palaeopiezometry. If crystal orientations can be mapped across the microstructure and the differential stress measured or inferred, then the scalars τ^s and m^s can be mapped across the microstructure.

To determine which of the calcite slip systems could potentially be activated by the palaeostresses, we transform the normalised stress tensor, $\hat{\boldsymbol{\sigma}}$, in Equation (6), into the crystal coordinate system of each measured orientation and compute m^s for each slip system. This stress tensor, $\hat{\boldsymbol{\sigma}}$, and Schmid tensor, \mathbf{m}^s , allow calculation of m^s by Equation (4). Values of m^s are multiplied by σ_{diff} to calculate the corresponding shear stress, τ^s , resolved on each slip system according to Equation (2). In crystals with multiple symmetrically equivalent variants of each slip/twin system, such as calcite, the variant with the highest value of m^s will slip/twin at the lowest applied stresses.

Once the Schmid factor and resolved shear stress for each slip system have been calculated, it is necessary to assess whether the applied stress was sufficient to activate dislocation glide, i.e., whether $\tau^s > \tau_c^s$. The experimental work on calcite single crystals and data compilation of De Bresser and Spiers (1993, 1997) established the operative calcite slip and twinning systems and their absolute CRSSs over the temperature range 20–800 °C. Therefore, we take the values of τ_c for {e}-twinning and dislocation slip on the {r}- and {f}-planes, for temperatures of 200 °C and 300 °C, from De Bresser and Spiers (1997) (Table 2). These temperatures approximately correspond to the lower- and upper-bounds for temperature constrained by the geological context (Section 2), for the occurrence of twinning and dynamic recrystallisation respectively in sample EM1. We use values of τ_c for the variant of the {f} slip system active at ≤ 300 °C (i.e., $\{\bar{1}012\}\langle 2\bar{2}01\rangle$), rather than the variant active at ≥ 500 °C (i.e., $\{\bar{1}012\}\langle \bar{1}01\bar{1}\rangle$) in the experiments of De Bresser and Spiers (1997). These experiments demonstrated that values of τ_c for calcite slip systems depend little on strain rate (stress exponents in the range 5.3–42.6), which reduces the uncertainty associated with applying them to analyse deformation that occurred at lower strain rates than the deformation experiments. The range of values of τ_c for slip on the {r} system at 300 °C, reported by De Bresser and Spiers (1997), is on the order of 20 MPa. As this range is smaller than the uncertainties of the palaeopiezometric stress estimates for the nature samples (30–35 MPa, Table 1, Rutter et al., 2007), we consider only the best-fit values of τ_c at each temperature, interpolated from the fits reported by De Bresser and Spiers (1997), to make simple first-order comparisons. From the critical resolved shear stresses constrained by experiments (De Bresser and Spiers, 1997) and from the applied differential stresses constrained by palaeopiezometry (Rutter et al., 2007), we compute the minimum value of m^s (i.e. m_{min}) necessary to initiate twinning or dislocation glide on each system by

$$m_{\text{min}} = \tau_c / \sigma_{\text{diff}}. \quad (7)$$

By computing maps of m^s , we are able to determine which grains have $m > m_{\text{min}}$ (and $\tau^s > \tau_c^s$) and therefore estimate the area fraction of grains that can deform by each deformation mode under the applied palaeostress conditions. We also perform this analysis for applied stresses throughout the range 1–250 MPa to explore the effects of increasing stress acting on the mapped microstructure at 300 °C and

200 °C. An MTEX script to carry out these procedures is included as [Supplementary Material](#).

An important caveat to the analysis described here is that the stress state would need to be homogeneous throughout the material for the point-by-point Schmid factors to be reliably accurate. However, micromechanical models of viscoplastic deformation that explicitly account for detailed microstructures suggest that stress and strain vary significantly among grains and are even distributed heterogeneously within grains (e.g. Pokharel et al., 2014). Heterogeneous distributions of stress and strain arise due to the elastic and plastic anisotropy of individual grains and local grain-grain interactions. Such heterogeneities have been recently observed in experimentally deformed Carrara marble (Quintanilla-Terminel and Evans, 2016). Thus, rather than interpreting the behaviour of specific individual points or grains, we take the approach of considering the distribution of Schmid factors and predicted slip/twin system activity over ~2500 grains, providing an averaged estimate of the slip system activity across the bulk material. We suggest that these averaged values of slip system activity are more reliable than the results for individual grains displayed in the maps because the stress states averaged throughout the rock volume must equal the macroscopic applied stress state. The Schmid factor approach offers a simple method to consider a larger number of grains than would be possible using more advanced computational techniques that include stress heterogeneity.

During progressive deformation, Schmid factors define only an instantaneous relationship between stress and crystal orientation, as ongoing crystal rotations continuously modify the Schmid factors for each slip system in aggregates deforming by dislocation glide. Therefore, Schmid factors calculated from the microstructure of an exhumed rock indicate which slip systems would have been well aligned for dislocation glide during the next increment of slip (which *ipso facto* never occurred). In contrast, use of mapped Schmid factors to interpret prior deformation that led to formation of the observed microstructure is more complex and requires additional assumptions/constraints regarding microstructural evolution (particularly grain rotations) or steady state. Therefore, Schmid factor analysis is well suited to our application, in which the mylonitic microstructure records a snapshot formed at ~300 °C as the dislocation-mediated processes that formed it ceased to operate, and in which our aim is to investigate the controls on the subsequent evolution of deformation processes.

4. Results

The measured CPO is consistent with the inference of simple shear deformation. Calcite {c}, {e} and {r} poles are clustered in point maxima near the foliation normal, whereas the twin and slip directions are weakly girdled with superimposed point maxima close to the lineation direction (Fig. 3). The CPO of {f} planes is weak, with three low intensity maxima (Fig. 3b).

Crystallographic misorientation data indicate that relatively few subgrain boundaries with misorientations in the range 1–10° are present (Fig. 4a), but the inverse pole figure of misorientation axes demonstrates that those subgrain boundaries that are present have rotation axes parallel to the $\alpha(11\bar{2}0)$ directions (Fig. 4b). The map of local misorientations scaled from 0–1.5° reveals the presence of abundant low-angle misorientations of ~1° (Fig. 4a). These misorientations are arranged in networks of low-angle subgrain boundaries and regions of more distributed lattice curvature. The portions of grains close to grain boundaries have greater local misorientation relative to the interior, representing higher dislocation densities, than grain interiors (Fig. 4a,d). The visible microstructure indicates that the measurements are generally above the background noise level, despite the small misorientation angles. Crystallographic vorticity axes are generally aligned sub-perpendicular to both the lineation and foliation normal, consistent with dominantly simple shear (Fig. 4c; Michels et al., 2015). This observation provides independent support for our choice of stress

state (i.e. Equation (6)) used for Schmid factor analysis.

Maps of Schmid factor show grain-by-grain variations in the maximum Schmid factor of each family of slip systems (Fig. 5). Each family of slip systems exhibits a wide range of Schmid factors within the map area (Fig. 5). The probability densities of Schmid factors exhibit similar general form between each slip system, being skewed towards high Schmid factors. The distribution describing Schmid factors for slip on {f}-planes is most heavily skewed towards high values (Fig. 5). Schmid factors vary between twins and host grains, evident as stripes of different Schmid factor. More subtle variations in Schmid factor are apparent across subgrain boundaries.

The apparent proportions of grains that can deform by each slip/twin system vary across the temperature and stress ranges within which deformation is inferred to have taken place (Figs. 6–8). At 300 °C and a piezometric stress of 98 MPa, none of the grains can deform by {f}-slip because τ_c (52 MPa) is greater than 0.5 of the applied stress (Figs. 6 and 8a, Table 2). However, within the upper-bound uncertainty of the stress estimate, up to 29% of the microstructure can deform by {f}-slip (Fig. 8a). Within the stress uncertainty, 63 + 18/–39% can deform by {r}-slip and 100% can deform by {e}-twinning (Figs. 6 and 8a). At 200 °C and the higher stress conditions estimated from twinning incidence, 39 + 17/–25% should be able to deform by {f}-slip and 72 + 7/–10% should be able to deform by {r}-slip (Figs. 7 and 8b). Again 100% of the grain area exceeds the critical resolved shear stress for {e}-twinning (Figs. 7 and 8b).

5. Discussion

5.1. Effects of changing temperature and stress on slip system activity

This study constitutes a detailed examination of the microstructure of a single sample of marble, EM1, deformed by dislocation glide and twinning whilst the Pangong Metamorphic Complex, within which it was situated, was exhumed through the frictional-viscous transition zone at temperatures of approximately 200–300 °C around 7–8 Ma (Rutter et al., 2007; Wallis et al., 2013, 2016b). Although this sample represents only a small volume of the fault zone material, the surrounding rocks, which include a wide range of fault rock types formed under varied conditions, provide a well-documented context (Rutter et al., 2007) in which to interpret the changing styles of deformation in both sample EM1 and the unit as a whole (Figs. 1 and 2). In particular, the frictional fault rocks, i.e. marble cataclasites and clay-rich gouge, are more spatially localised than the mylonitic marbles that they overprint (Fig. 1; Rutter et al., 2007). Therefore, microstructural evidence for earlier deformation mechanisms and processes, such as the recrystallised microstructure indicative of dislocation-mediated deformation in EM1, remains preserved and available for analysis, whilst the subsequent switch to frictional failure of the adjacent rocks can be inferred from the locally overprinting frictional fault rock types. The Kübler index of illite in the clay-rich gouge layer suggests that it formed at up to approximately 300 °C and therefore closely post-dated mylonitisation, which ceased at approximately 300 °C (Fig. 2; Rutter et al., 2007). As such, formation of the gouge was broadly coincident with twinning in the mylonitic marbles, which occurred at approximately 200–250 °C (Fig. 2, Burkhard, 1993). Similarly, the mylonitic marbles are fragmented and overprinted by cataclasites in a zone tens of metres wide adjacent to the gouge layer (Fig. 1; Rutter et al., 2007). The fragmented marbles contain relict microstructures indicative of partial dynamic recrystallisation by grain boundary migration prior to cataclasis (Rutter et al., 2007). Therefore, cataclasis must also have occurred after mylonitisation and been broadly coincident with, or more recent than, formation of the gouge layer and twinning in the mylonites (Fig. 2). As the mylonitic fabric of EM1 formed at temperatures similar to or only slightly above those at which frictional deformation commenced in the adjacent rocks, we infer that the mylonitic microstructure of the sample remained largely unmodified during subsequent

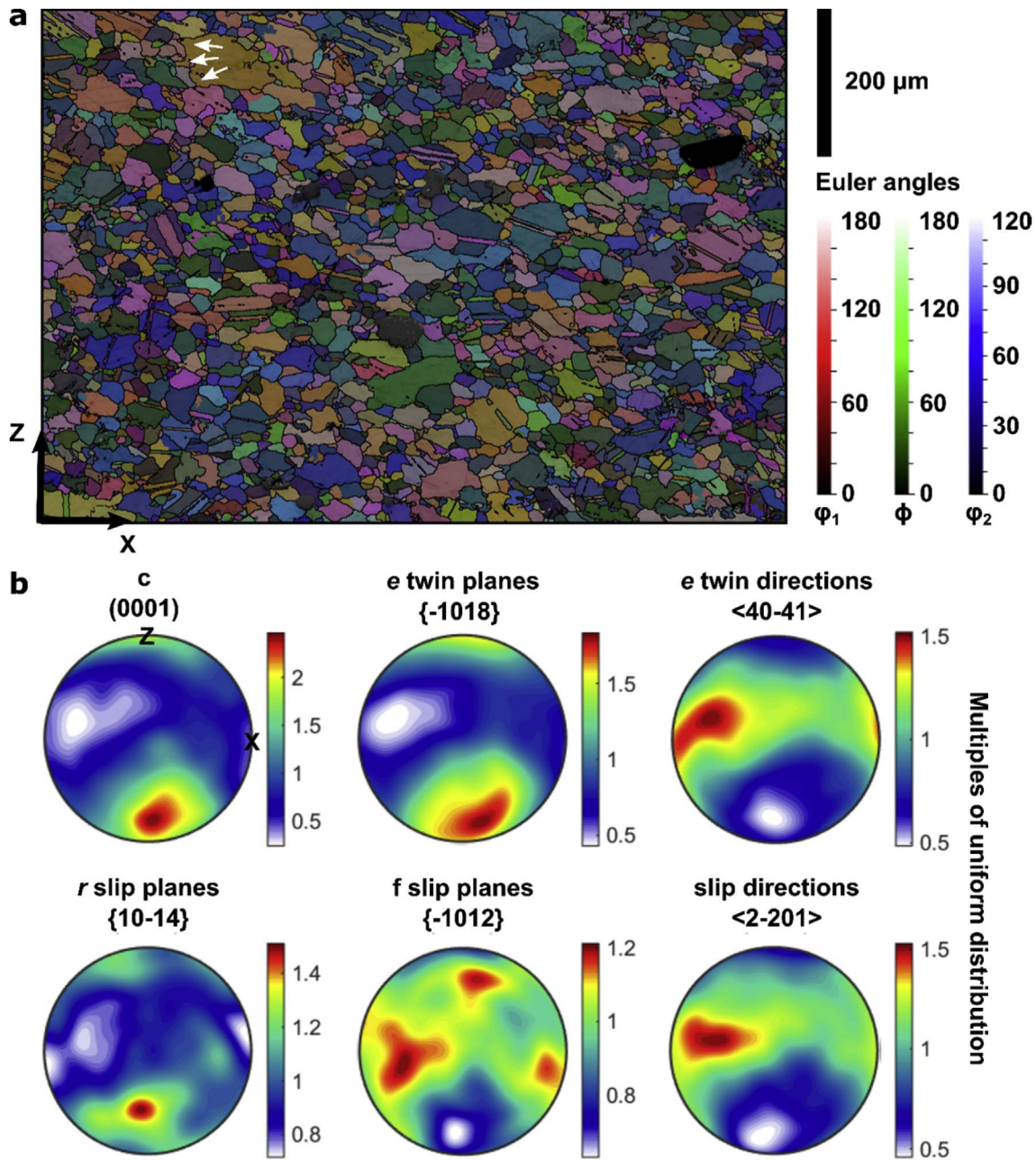


Fig. 3. Crystal orientation data from EBSD analysis of sample EM1. (a) Map of crystal orientations colour-coded using Euler angles in the convention of Bunge (1982), superimposed on a grey-scale map of diffraction pattern band contrast. Black lines mark boundaries of $\geq 10^\circ$ misorientation between adjacent pixels. White arrows indicate an example of a lobate and irregular grain boundary. (b) Lower hemisphere pole figures of crystal planes and directions relevant to the calcite slip and twin systems considered. X indicates the lineation and Z the foliation normal. Shear sense is top-to-right. (For interpretation of the references to colour in this figure legend, the reader is referred to the web version of this article.)

exhumation. We also note that EM1 is located close to the boundary between the mylonitic and fragmented marbles and therefore is well suited (in both spatial location and timing of formation of its deformation fabric) to recording the transition between dislocation-mediated and frictional deformation. These relationships allow us to examine one sample in detail whilst also considering the significance of the deformation processes in the evolution of the rock unit more widely.

The predicted changes in slip system activity in EM1 (Fig. 8) reflect the combined influence of changing stress and temperature conditions as the rock was exhumed. The decrease in temperature from 300 °C to 200 °C increases values of τ_c by factors of 1.5–1.9 (Table 2), acting to inhibit dislocation glide. However, palaeopiezometric estimates suggest that, at the same time, the applied stress increased by a factor of ~2.1

(Rutter et al., 2007). As a result, a greater fraction of the microstructure appears to have potential to deform by dislocation glide at 200 °C and 210 ± 30 MPa than at 300 °C and 98 ± 35 MPa (Figs. 6–8). This effect is particularly pronounced for {f}-slip, which has the highest τ_c . The 98 ± 35 MPa applied stress at 300 °C is generally insufficient for slip on {f}-planes, whereas, at 200 °C and 210 ± 30 MPa, 39 + 17/–25% of the microstructure exceeds τ_c for {f}-slip (Fig. 8). However, these findings are superficially at odds with other microstructural and structural features that indicate dislocation activity was greater at higher temperature. Within the sample, dynamically recrystallised grains formed under the lower stress, higher temperature conditions, and were not overprinted by further dynamic recrystallisation under the subsequent higher stress, lower temperature conditions (Fig. 2; Rutter et al., 2007). More widely in the rock unit, the mylonitic textures

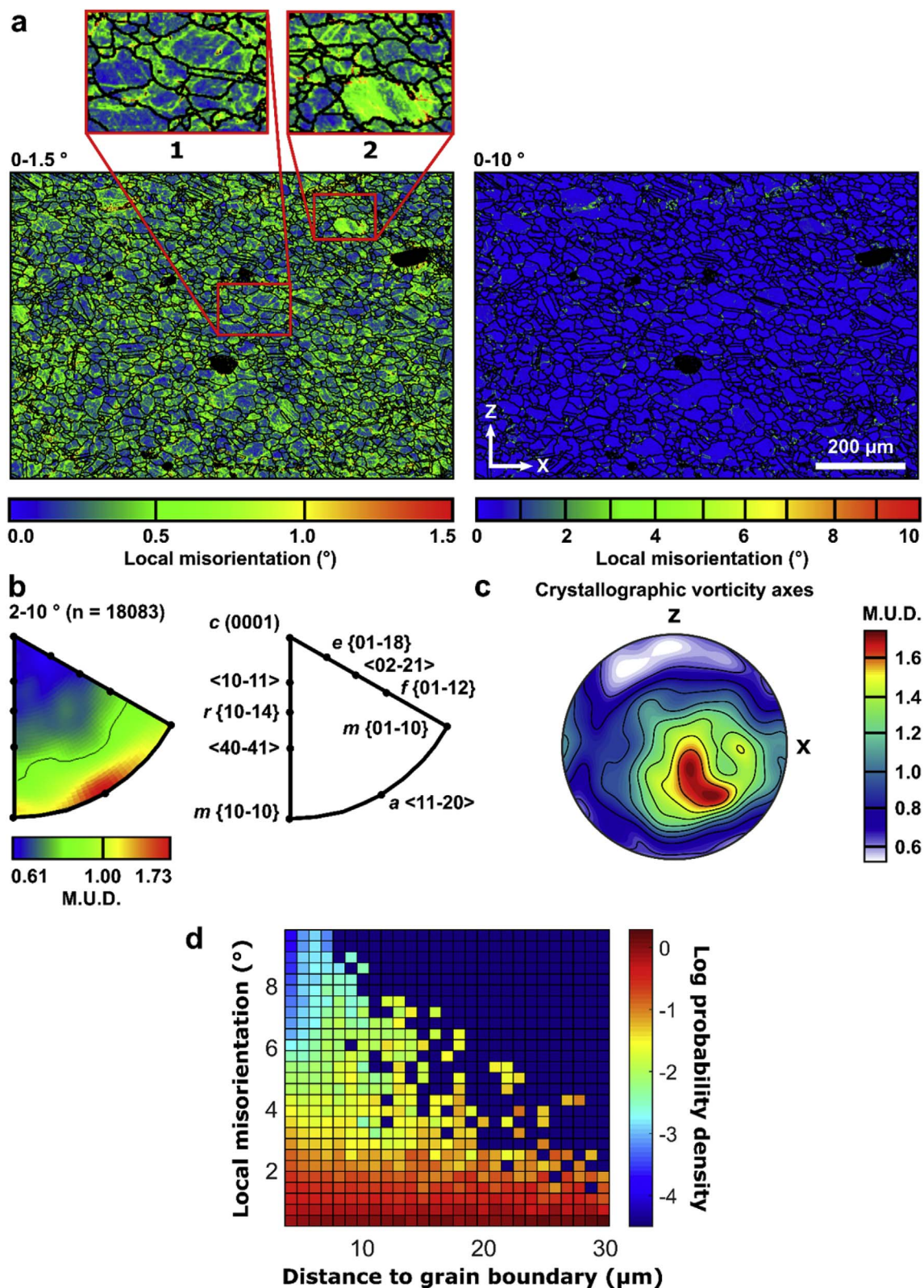


Fig. 4. Misorientation analysis of EM1. (a) Maps of local misorientation within 3×3 pixel kernels, scaled for two ranges of misorientation angle. Grain and twin boundaries are overlaid as black lines. Region 1 exhibits higher values of misorientation concentrated near grain boundaries. Region 2 shows both subgrain boundaries (top left) and more widespread misorientation (lower right). (b) Inverse pole figure presents the orientation of misorientation axes of subgrain boundaries in the crystal reference frame. (c) Stereoplot illustrating contoured crystallographic vorticity axes (one axis per grain), determined using the method of principal geodesic analysis of intragranular dispersion (Michels et al., 2015). X indicates the lineation and Z the foliation normal. (d) Probability density functions (PDFs) of local misorientation in $1 \mu\text{m}$ bins of Euclidean distance to grain boundary (including twin boundaries) within the 2-D EBSD map plane, i.e. each column is a different PDF. This plotting approach addresses the bias of having different numbers of points at each distance by allowing PDFs to be compared between different distances. Local misorientation was calculated within a 3×3 pixel kernel. Only points at distances $> 3 \mu\text{m}$ from a grain boundary are plotted to avoid processing artefacts in kernels that include boundaries. Grain boundaries were defined as $> 10^\circ$ misorientation.

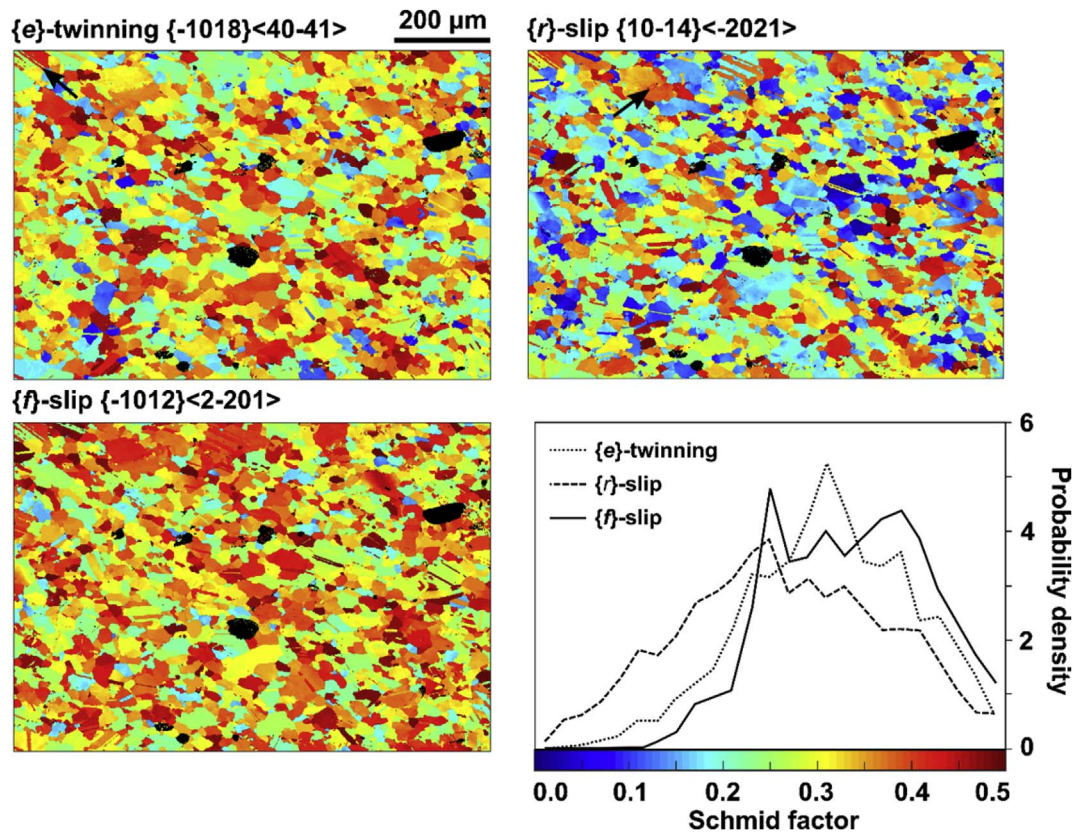


Fig. 5. Maps and probability density plots of Schmid factor for each calcite slip/twin system. Probability densities were calculated for bins of 0.02 width. The black arrow in the upper-left of the map of Schmid factor for {e}-twinning indicates an example of changes in Schmid factor across twin boundaries. The black arrow in the upper-left of the map of Schmid factor for {r}-slip indicates an example of changes in Schmid factor across a subgrain boundary.

formed at the higher temperatures are overprinted by cataclasites and gouges formed at similar and lower temperatures (Fig. 2; Rutter et al., 2007). One possible explanation for the discrepancy between the predictions of slip system activity (Fig. 8) and the observed (micro)structural evolution is that the stresses predicted from twinning incidence by the palaeopiezometer of Rowe and Rutter (1990) are inaccurate. This method for estimating past stresses is fully empirical and lacks a detailed microphysical basis often used to support application of laboratory-derived relationships to natural contexts. However, the predicted stresses would have to be in error by approximately a factor of two, or approximately 100 MPa, to preclude slip on the {r} system in well oriented grains (Fig. 8). Therefore, in the following section, we discuss in more detail the evolution of deformation processes as the rock cooled during exhumation to explore the possibility that microphysical processes are responsible for lack of significant dislocation glide under the low temperature and high stress conditions.

5.2. Evolution of deformation mechanisms during exhumation through the frictional-viscous transition zone

Calcite microstructures in EM1 (this study) and the other samples reported by Rutter et al. (2007) include lobate grain boundaries (Figs. 3 and 4), porphyroclasts with fine grained mantles (Rutter et al., 2007), and subgrain boundaries (Fig. 4). These microstructural observations indicate deformation by dislocation motion, accompanied by dynamic recrystallisation due to grain boundary migration and (to a lesser extent) subgrain rotation (Figs. 3 and 4; Rutter et al., 2007). Crosscutting relationships and contrasting palaeopiezometric estimates indicate that these microstructures formed close to the upper bound temperature of 310 ± 20 °C for EM1, constrained by the (now partially overprinted) equilibrium grainsize (Fig. 2; Rutter et al., 2007).

The general scarcity of subgrain boundaries with misorientations of

several degrees or more (Fig. 4) indicates that dislocation climb was limited at these temperatures and/or that recovery of intracrystalline strain occurred by other processes, such as cross-slip, dislocation annihilation or climb into high-angle grain boundaries and grain-boundary migration (De Bresser and Spiers, 1990; Liu and Evans, 1997). Misorientation analysis of the few subgrain boundaries that are present indicates that they mostly involve lattice rotations around axes parallel to $a\langle 11\bar{2}0 \rangle$. Bestmann and Prior (2003) demonstrated that misorientation axes parallel to $\langle a \rangle$ in calcite cannot represent twist boundaries due to the lack of appropriate screw dislocation types in calcite. They also suggested that a precisely defined misorientation axis could result from coupled activity of glide in two co-planar directions, but that this is unlikely in general as it requires an equal contribution from both slip directions. Rather, the misorientation axes are consistent with tilt boundaries constructed of edge dislocations on the $r\{10\bar{1}4\}\langle 2\bar{2}01 \rangle$ or $f\{10\bar{1}2\}\langle 10\bar{1}1 \rangle$ slip systems (Bestmann and Prior, 2003). However, as $f\{10\bar{1}2\}\langle 10\bar{1}1 \rangle$ is the high temperature form of {f}-slip, active above 500 °C in the experiments of De Bresser and Spiers (1997), dislocations on this slip system are unlikely to have formed the subgrain boundaries in EM1. Edge dislocations on the low temperature {f}-slip system, $f\{10\bar{1}2\}\langle 2\bar{2}01 \rangle$, which we have analysed here, do not generate lattice rotations around $\langle a \rangle$ and therefore also cannot form the subgrain boundaries in EM1. We infer therefore that the subgrain boundaries are constructed of edge dislocations on the $r\{10\bar{1}4\}\langle 2\bar{2}01 \rangle$ slip system. This interpretation is consistent with the estimate that ~63–72% of the microstructure had sufficient resolved shear stress for slip on $r\{10\bar{1}4\}\langle 2\bar{2}01 \rangle$ across the range of conditions investigated (Fig. 8). These conclusions are similar to those reached by Bestmann and Prior (2003), who investigated calcite deformed at temperatures in the range ~300–350 °C.

The marble mylonites are sequentially overprinted by more localised marble cataclasite and the clay-bearing gouge zone (Figs. 1 and 2;

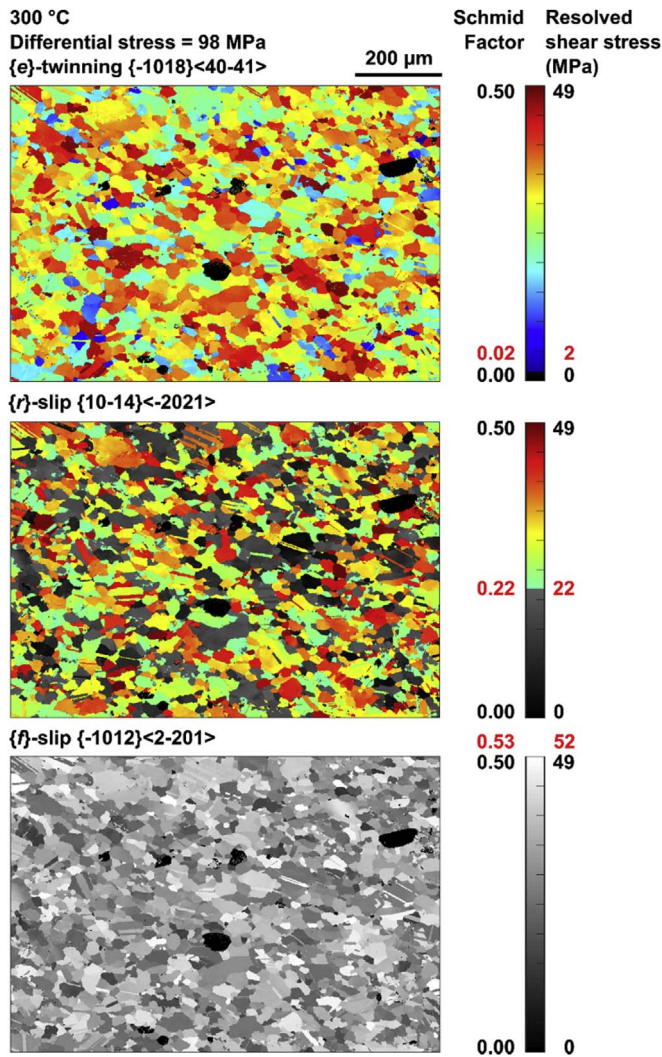


Fig. 6. Maps of grains that exceed the minimum Schmid factor necessary to initiate twinning or dislocation glide at 300 °C and the stress determined from dynamically recrystallised grain size. The minimum Schmid factor and corresponding critical resolved shear stress are marked in red beside the colour bar. Areas above and below this threshold are represented by colour-scale and grey-scale respectively. (For interpretation of the references to colour in this figure legend, the reader is referred to the web version of this article.)

Rutter et al., 2007). These cross-cutting relationships and associated microstructures indicate that, as temperature decreased during exhumation, stress increased sufficiently that the frictional failure strength of the rock was exceeded. This onset of frictional deformation occurred after mylonitisation at ~ 300 °C and before, or broadly coincident with, development of the preserved set of twins in the marble (200–250 °C, Fig. 2; Rutter et al., 2007). We provide additional insight through our Schmid factor analysis, which demonstrates that the calcite would still have had sufficient resolved shear stress for dislocation glide in most crystal orientations if CRSS values taken from the yield points in single crystal experiments are applicable to the natural microstructure. The resolved shear stress appears sufficient for considerable dislocation glide even at the lower temperatures of 200–250 °C (Figs. 7 and 8) at which only twinning and frictional failure occurred (Rutter et al., 2007). In fact, the predictions of slip system activity (Fig. 8) indicate that the applied shear stress would have to have been approximately half of the value measured by twinning incidence to de-activate {r}-slip in a significant portion of the microstructure.

It is important to note that the τ_c values upon which this analysis is based were experimentally determined for relatively low strains of just

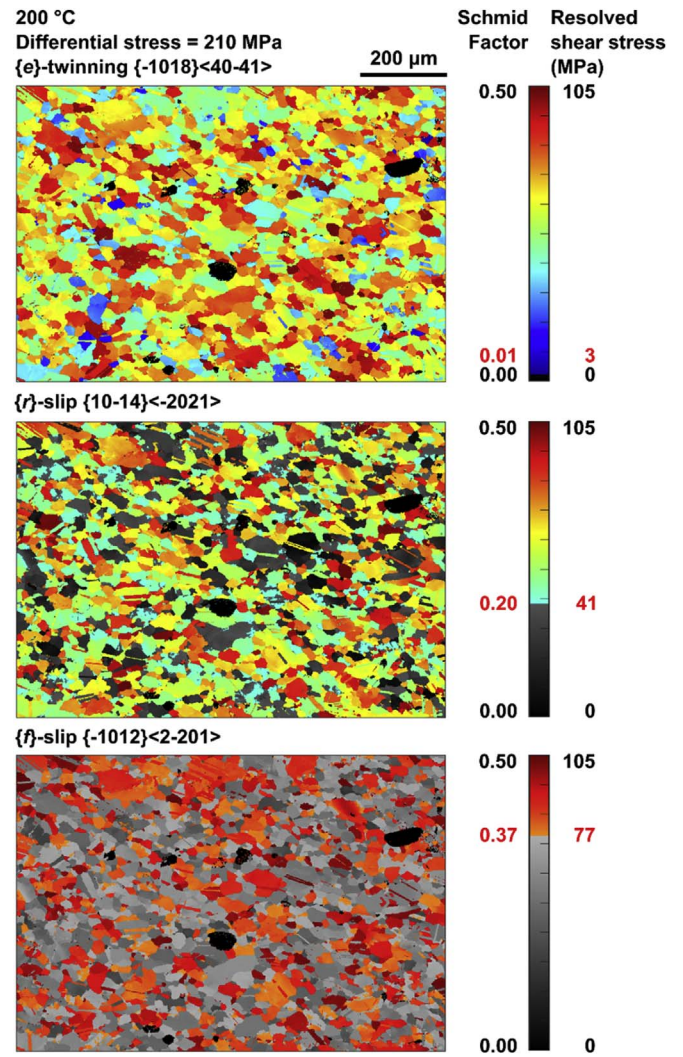


Fig. 7. Maps of grains that exceed the minimum Schmid factor necessary to initiate twinning or dislocation glide at 200 °C and the stress determined from twinning incidence. The minimum Schmid factor and corresponding critical resolved shear stress are marked in red beside the colour bar. Areas above and below this threshold are represented by colour-scale and grey-scale respectively. (For interpretation of the references to colour in this figure legend, the reader is referred to the web version of this article.)

a few percent ($\leq 4.3\%$, De Bresser and Spiers, 1997). De Bresser and Spiers (1997) recognized significant strain hardening in their experiments, such that the CRSS obtained from yield point stresses effectively places a minimum bound on the resolved shear stress required for further dislocation glide on the corresponding slip system at higher strains. This observation led De Bresser and Spiers (1997) to suggest that strain hardening on the first slip system to activate (i.e., {r}-slip) could lead to a strain-induced transition to a different dominant slip system (e.g., {f}-slip).

Strain hardening in calcite during cooling is likely the result of a reduction in the efficiency of thermally activated intracrystalline strain recovery processes such as cross slip or dislocation climb into either static or migrating twin, subgrain, and grain boundaries (Rutter, 1974; De Bresser and Spiers, 1990; Kennedy and White, 2001). As a result, dislocation interactions and long-range stress fields associated with accumulations of blocked dislocations would have inhibited further dislocation glide (Fleck et al., 1994; Renner et al., 2002). Two lines of microstructural evidence support this interpretation. The widespread occurrence of subgrain boundaries with low misorientation angles of approximately 0.5 – 1.0° (Fig. 4) suggests that significant dislocation

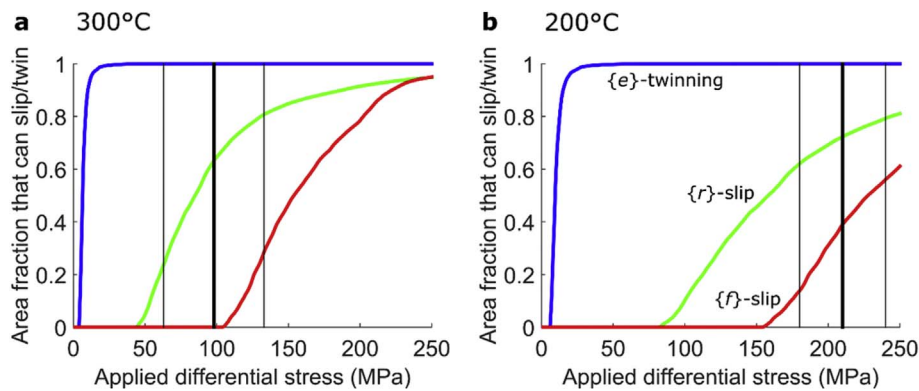


Fig. 8. Area fraction of grains in mapped microstructure that can deform by twinning/dislocation glide at (a) 300 °C and (b) 200 °C, under applied differential stresses ranging from 0–250 MPa. The stress estimates are determined from (a) dynamically recrystallised grain size (at ~300 °C) and (b) twinning incidence (at 200–250 °C) and are marked by vertical bold black lines with uncertainties marked by fine black lines.

content is present but that dislocations could not organise into lower-energy structures. Similarly, misorientation angles, and hence dislocation content, generally increase towards grain boundaries (Fig. 4) suggesting that dislocation climb into boundaries and grain-boundary migration were relatively inefficient compared to the rate of dislocation accumulation.

Renner et al. (2002) suggested that calcite commonly exhibits a Hall-Petch relationship whereby strength increases with decreasing grain size because back-stresses from dislocations accumulated near grain boundaries inhibit further dislocation glide. This model is consistent with the microstructural observations (orientation gradients generally increasing towards grain boundaries) and mechanical inferences (occurrence of strain hardening) of this study. Kennedy and White (2001) reached similar conclusions based on observations of calcite naturally deformed at relatively low temperatures of 150–250 °C. Microstructures in their samples indicated that coarse-grained vein calcite that crystallised with low dislocation densities was able to deform by dislocation glide, whereas finer-grained mylonitic matrix exhibited high densities of tangled dislocations and was interpreted to have strain-hardened. We suggest therefore that the transition from dislocation-mediated flow to frictional failure was promoted by work hardening due to low efficiency of recovery processes, particularly slow climb into grain boundaries, rather than simply the temperature-dependency of critical resolved shear stresses, as the rocks cooled during exhumation. This inference is consistent with experimental observations that strain hardening is more pronounced at lower temperatures for both single crystals (De Bresser and Spiers, 1993; 1997) and aggregates (Rutter, 1974). The predictions of slip system activity (Fig. 8) suggest that strain hardening must have imposed additional resistance to glide of at least tens of MPa to prevent large fractions of the microstructure deforming by {r}-slip.

Microstructures indicative of frictional deformation are preserved within both the cataclastic marbles and the phyllosilicate-rich gouge band (Fig. 1; Rutter et al., 2007). As Quaternary earthquakes of magnitude 7+ are recorded by offset alluvial fans and debris flows within 2 km of the sample site (Brown et al., 2002; Rutter et al., 2007), it is pertinent to consider the extent to which the exhumed cataclastic fault rocks record seismogenic processes as an analogue for those occurring at depth. Phyllosilicate-rich gouges typically exhibit velocity-strengthening behaviour and therefore are unfavourable in general for nucleation of earthquake ruptures (Ikari et al., 2011). However, carbonate rocks exhibit strong velocity weakening (Han et al., 2010), and therefore the fragmented marble band was likely capable of nucleating unstable earthquake ruptures whilst at depth. In this case, one important consequence of strain hardening may be to result in the onset of seismogenic deformation at the structural levels at which rocks are exhumed and cooled from ~300 °C to ~200–250 °C. We suggest that the processes recorded in the presently exposed fault rocks of the Pangong strand are likely analogous to those occurring at depth, where similar rocks of the PMC continue to be exhumed through the frictional-viscous

transition zone.

In the case of the KFZ, cooling through the frictional-viscous transition zone was due to ongoing deformation during erosional exhumation (Wallis et al., 2016b). However, the processes documented in this study may also be important in controlling transitions in deformation mechanism and the onset of seismogenic behaviour in other tectonic settings. In particular, carbonate units are commonly dissected by extensive normal fault systems in which tectonic exhumation of footwalls may contribute to cooling (Smith et al., 2011; Cowie et al., 2017). The processes of strain hardening leading to frictional failure may be important controls on the depth of seismicity and strength of the extending mid-crust in such settings. An implication of this finding is that the depth extent of the dominantly frictional upper crust, where earthquakes typically nucleate, potentially varies in both space and time in response to the evolving strain state of rocks in the mid-crust.

5.3. Schmid factor analysis as a tool for analysing crystal plasticity

Schmid-factor analysis provides several useful insights in addition to those that can be gained from more commonly used methods of slip system analysis. Schmid factor maps provide an extension of common CPO analysis by allowing populations of crystal orientations to be readily related directly to specific microstructural elements (e.g. Figs. 5–7). This approach is similar to plotting EBSD maps colour-coded using inverse pole figures, except that Schmid factor maps consider the complete crystallography (i.e. angular relationships involving both the slip direction and slip plane normal) rather than individual crystal directions, and relate this explicitly to a stress state of interest (which is often only implied in other approaches).

Schmid factor mapping is also the first step to more detailed quantitative analysis of slip system activity, which requires a range of geological (e.g. stress and temperature) and experimental (e.g. CRSS and strain rate sensitivity) constraints. In these respects, calcite is ideal, whereas other common rock forming minerals may present additional challenges. For example, the slip systems of quartz are relatively well constrained and quartz slip system analysis is widely applied in studies of crustal deformation (e.g. Law et al., 1990; Lloyd et al., 1997; Morales et al., 2014). However, single crystals of quartz exhibit complex yield behaviour, with strength dependent not only on temperature but also strain rate and intragranular water content (Hobbs et al., 1972). Consequently, comprehensive measurements of slip system strength, such as those available for calcite (De Bresser and Spiers, 1997), are not currently available for quartz. As a result of these limitations, although it is possible to calculate Schmid factors for quartz slip systems, it is not yet possible to infer which slip systems have sufficient resolved shear stress for slip. Similar detailed considerations must be applied to other common rock-forming minerals.

More generally, Schmid factor analysis can require a range of assumptions, depending on the application, which must be critically evaluated. In the present work we are concerned with why dislocation

activity ceased at the time that the preserved mylonitic microstructure was formed. In this respect, Schmid factor analysis is highly appropriate because it constrains which slip systems were well aligned for dislocation glide during a hypothetical *future* increment of dislocation-mediated strain. However, a common objective of other rock deformation studies is to interpret how an observed microstructure formed in the first place. Schmid factors calculated for specific points/grains in a mapped microstructure will generally not equal those present during *prior* deformation that lead to formation of the observed microstructure due to microstructural evolution (e.g., grain rotation, grain boundary migration). In some instances, this limitation might be overcome by assuming that the microstructure had ‘on average’ reached a steady state, in combination with analysing Schmid factor distributions over a large portion of the microstructure. However, microstructural steady state, and in particular steady-state CPO, can require shear strains of several hundred percent and can be difficult to prove (Skemer and Hansen, 2016). Averaging over large portions of the microstructure also provides the benefit of reducing the influence of inter- and intra-granular stress heterogeneities. Such heterogeneities have been predicted by numerical modelling (e.g., Pokharel et al., 2014; Lebensohn and Needleman, 2016) and documented in geological crystalline aggregates, including calcite (Quintanilla-Terminel and Evans, 2016) and quartz (Chen et al., 2015), and even in single crystals of olivine (Wallis et al., 2017). Therefore, it is important to map Schmid factors over a sufficiently large portion of the microstructure that the averaged internal stress state can be reasonably expected to have approached the macroscopic externally applied stress state during deformation. Notwithstanding these caveats, the present study demonstrates that Schmid factor analysis can provide geologically relevant information, if used in conjunction with appropriate objectives and geological constraints.

6. Conclusions

Schmid factor analysis indicates that calc-mylonites in the Pangong strand of the KFZ deformed primarily by dislocation glide on $r\{10\bar{1}4\}\langle 201 \rangle$ at $\sim 300^\circ\text{C}$ and 98 ± 35 MPa differential stress (Rutter et al., 2007) and by $e\{1018\}\langle 40\bar{1}1 \rangle$ twinning at similar and lower temperatures. In contrast, the critical resolved shear stress for dislocation glide on $f\{1012\}\langle 2\bar{2}01 \rangle$ precluded this slip system from activating in the majority of grains under the same conditions. Deformation within the Karakoram Fault Zone continued as the rocks cooled during exhumation, resulting in hardening of the calc-mylonites and thereby leading to a transition from crystal plastic to frictional deformation mechanisms (Rutter et al., 2007; Wallis et al., 2013). One mechanism for such hardening is by the direct temperature effect of increasing critical resolved shear stresses of the active slip and twin systems (De Bresser and Spiers, 1997). However, Schmid factor analysis indicates that this alone was insufficient to induce frictional failure as a greater fraction of the microstructure apparently had sufficient resolved shear stress for dislocation glide at 200°C than at 300°C . Instead, microstructural observations, such as widespread low angle crystallographic misorientations, which increase towards grain boundaries, indicate that intracrystalline strain recovery was inefficient. Strain hardening, due to decreasing efficiency of recovery as temperature decreased, provides an additional hardening mechanism, which we interpret as having led to the onset of frictional and potentially seismogenic deformation in the rocks at this structural level. These findings highlight the importance of detailed understanding of the interplay of strain hardening and recovery processes for models of crystal plasticity, particularly at relatively low homologous temperatures where they impact the transition to frictional and potentially seismogenic deformation.

Acknowledgements

We thank Richard Phillips and Ernie Rutter for providing the sample

for this study, Cees Passchier for his editorial handling of the manuscript, and Hans de Bresser and Elisabetta Mariani for their reviews. We are grateful to Rick Law, Gordon Lister and Andrew Turner for helpful discussions. David Wallis and Lars Hansen acknowledge support from the Natural Environment Research Council grant NE/M000966/1. Data reported in this study are available on request from the corresponding author.

Appendix A. Supplementary data

Supplementary data related to this article can be found at <http://dx.doi.org/10.1016/j.jsg.2017.11.008>.

References

- Bachmann, F., Hielscher, R., Schaeben, H., 2010. Texture analysis with MTEX – free and open source software toolbox. *Solid State Phenom.* 160, 63–68. <http://dx.doi.org/10.4028/www.scientific.net/SSP.160.63>.
- Bestmann, M., Prior, D.J., 2003. Intragranular dynamic recrystallisation in naturally deformed calcite marble: diffusion accommodated grain boundary sliding as a result of subgrain rotation recrystallisation. *J. Struct. Geol.* 25, 1597–1613. [http://dx.doi.org/10.1016/S0191-8141\(03\)00006-3](http://dx.doi.org/10.1016/S0191-8141(03)00006-3).
- Bestmann, M., Prior, D.J., Grasemann, B., 2006. Characterisation of deformation and flow mechanics around porphyroclasts in a calcite marble ultramylonite by means of EBSD analysis. *Tectonophysics* 413, 185–200. <http://dx.doi.org/10.1016/j.tecto.2005.10.044>.
- Boutonnet, E., Leloup, P.H., Arnaud, N., Paquette, J.-L., Davis, W.J., Hattori, K., 2012. Synkinematic magmatism, heterogeneous deformation, and progressive strain localisation is a strike-slip shear zone: the case of the right-lateral Karakorum fault. *Tectonics* 31, TC4012. <http://dx.doi.org/10.1029/2011TC003049>.
- Brown, E.T., Bendick, R., Bourlès, D.L., Gaur, V., Molnar, P., Raisbeck, G.M., Yiou, F., 2002. Slip rates of the Karakorum fault, Ladakh, India, determined using cosmogenic ray exposure dating of debris flows and moraines. *J. Geophys. Res.* 107 (B9), 2192. <http://dx.doi.org/10.1029/2000JB00100>.
- Bunge, H., 1982. *Texture Analysis in Materials Science: Mathematical Models*. Butterworths, London, pp. 614.
- Burkhard, M., 1993. Calcite twins, their geometry, appearance and significance as stress-strain markers and indicators of tectonic regime: a review. *J. Struct. Geol.* 15, 351–368. [http://dx.doi.org/10.1016/0191-8141\(93\)90132-T](http://dx.doi.org/10.1016/0191-8141(93)90132-T).
- Chen, K., Kunz, M., Tamura, N., Wenk, H.-R., 2015. Residual stress preserved in quartz from the San Andreas fault observatory at depth. *Geology* 43, 219–222. <http://dx.doi.org/10.1130/G36443>.
- Covey-Crump, S.J., Rutter, E.H., 1989. Thermally induced grain growth of calcite marbles on Naxos Island, Greece. *Contrib. Mineral. Petrol.* 101, 69–86. <http://dx.doi.org/10.1007/BF00387202>.
- Cowie, P.A., Phillips, R.J., Roberts, G.P., McCaffrey, K., Zijerveld, L.J.J., Gregory, L.C., Faure Walker, J., Wedmore, L.N.J., Dunai, T.J., Binnie, S.A., Freeman, S.P.H.T., Wilcken, K., Shanks, R.P., Huismans, R.S., Papanikolaou, I., Michetti, A.M., Wilkinson, M., 2017. Orogen-scale uplift in the central Italian Apennines drives episodic behaviour of earthquake faults. *Sci. Rep.* 7, 44858. <http://dx.doi.org/10.1038/srep44858>.
- De Bresser, J.H.P., Spiers, C.J., 1990. High temperature deformation of calcite single crystals by r^+ and f^+ slip. In: Knipe, R.J., Rutter, E.H. (Eds.), *Deformation Mechanisms, Rheology and Tectonics*, vol. 54. Geological Society, London, pp. 285–298. <http://dx.doi.org/10.1144/GSL.SP.1990.054.01.25>. Special Publications.
- De Bresser, J.H.P., Spiers, C.J., 1993. Slip systems in calcite single crystals deformed at $300\text{--}800^\circ\text{C}$. *J. Geophys. Res.* 98, 6397–6409. <http://dx.doi.org/10.1029/92JB02044>.
- De Bresser, J.H.P., Spiers, C.J., 1997. Strength characteristics of the r , f , and c slip systems in calcite. *Tectonophysics* 272, 1–23. [http://dx.doi.org/10.1016/S0040-1951\(96\)00273-9](http://dx.doi.org/10.1016/S0040-1951(96)00273-9).
- Farla, R.J.M., Fitz Gerald, J.D., Kokkonen, H., Halfpenny, A., Faul, U.H., Jackson, I., 2011. Slip system and EBSD analysis on compressively deformed fine-grained polycrystalline olivine. In: Prior, D.J., Rutter, E.H., Tatham, D.J. (Eds.), *Deformation Mechanisms, Rheology and Tectonics: Microstructures, Mechanics and Anisotropy*, vol. 360. Geological Society, London, pp. 225–235. <http://dx.doi.org/10.1144/SP360.13>. Special Publications.
- Fleck, N.A., Muller, G.M., Ashby, M.F., Hutchinson, J.W., 1994. Strain gradient plasticity: theory and experiment. *Acta Metal. Mater.* 42, 475–487. [http://dx.doi.org/10.1016/0956-7151\(94\)90502-9](http://dx.doi.org/10.1016/0956-7151(94)90502-9).
- Han, R., Hirose, T., Shimamoto, T., 2010. Strong velocity weakening and powder lubrication of simulated carbonate faults at seismic slip rates. *J. Geophys. Res.* 115, B03412.
- Handy, M.R., Hirth, G., Bürgmann, R., 2007. Continental fault structure and rheology from the frictional-viscous transition downward. In: Handy, M.R., Hirth, G., Hovius, N. (Eds.), *Tectonic Faults – Agents of Change on a Dynamic Earth*, vol. 95. The MIT Press, Cambridge, Massachusetts, pp. 139–181 Dahlem Workshop Report.
- Hansen, L.N., Zimmerman, M.E., Kohlstedt, D.L., 2011. Grain boundary sliding in San Carlos olivine: flow law parameters and crystallographic-preferred orientation. *J. Geophys. Res.* 116, B08201. <http://dx.doi.org/10.1029/2011JB008220>.
- Hobbs, B.E., McLaren, A.C., Paterson, M.S., 1972. Plasticity of single crystals of synthetic quartz. In: Heard, H.C., Borg, I.Y., Carter, N.L., Rayleigh, C.B. (Eds.), *Flow and*

- Fracture of Rocks. American Geophysical Union, Washington D.C., pp. 29–53. <http://dx.doi.org/10.1029/GM016p0029>.
- Ikari, M.J., Marone, C., Saffer, D.M., 2011. On the relation between fault strength and frictional stability. *Geology* 39, 83–86. <http://dx.doi.org/10.1130/G31416.1>.
- Kennedy, L.A., White, J.C., 2001. Low-temperature recrystallisation in calcite: mechanisms and consequences. *Geology* 29, 1027–1030. [http://dx.doi.org/10.1130/0091-7613\(2001\)029<1027:LTRICM>2.0.CO;2](http://dx.doi.org/10.1130/0091-7613(2001)029<1027:LTRICM>2.0.CO;2).
- Law, R.D., Schmid, S.M., Wheeler, J., 1990. Simple shear deformation and quartz crystallographic fabrics: a possible natural example from the Torridon area of NW Scotland. *J. Struct. Geol.* 12, 29–45.
- Lebensohn, R.A., Needleman, A., 2016. Numerical implementation of non-local polycrystal plasticity using fast Fourier transforms. *J. Mech. Phys. Solids* 97, 333–351. <http://dx.doi.org/10.1016/j.jmps.2016.03.023>.
- Liu, M., Evans, B., 1997. Dislocation recovery kinetics in single-crystal calcite. *J. Geophys. Res.* 102, 24801–24809. <http://dx.doi.org/10.1029/97JB01892>.
- Lloyd, G.E., Farmer, A.B., Mainprice, D., 1997. Misorientation analysis and the formation and orientation of subgrain and grain boundaries. *Tectonophysics* 279, 55–78. [http://dx.doi.org/10.1016/S0040-1951\(97\)00115-7](http://dx.doi.org/10.1016/S0040-1951(97)00115-7).
- Mainprice, D., Bachmann, F., Hielscher, R., Schaebein, H., 2011. Calculating anisotropic physical properties from texture data using the MTEX open source package. In: Prior, D.J., Rutter, E.H., Tatham, D.J. (Eds.), *Deformation Mechanisms, Rheology and Tectonics: Microstructures, Mechanics and Anisotropy*, vol. 360. Geological Society, London, pp. 175–192. <http://dx.doi.org/10.1144/SP360.10>. Special Publications.
- Michels, Z.D., Kruckenburg, S.C., Davis, J.R., Tikoff, B., 2015. Determining vorticity axes from grain-scale dispersion of crystallographic orientations. *Geology* 43, 803–806.
- Morales, L.F.G., Lloyd, G.E., Mainprice, D., 2014. Fabric transitions in quartz via viscoplastic self-consistent modeling part I: axial compression and simple shear under constant strain. *Tectonophysics* 636, 52–69.
- Parsons, A.J., Law, R.D., Lloyd, G.E., Phillips, R.J., Searle, M.P., 2016. Thermo-kinematic evolution of the Annapurna-Dhaulagiri Himalaya, central Nepal: the composite orogenic system. *Geochim. Geophys. Geosys.* 17, 1511–1539. <http://dx.doi.org/10.1002/2015GC006184>.
- Phillips, R.J., Parrish, R.R., Searle, M.P., 2004. Age constraints on ductile deformation and long-term slip rates along the Karakoram fault zone, Ladakh. *Earth Planet. Sci. Lett.* 226, 305–319. <http://dx.doi.org/10.1016/j.epsl.2004.07.037>.
- Phillips, R.J., Searle, M.P., 2007. Macrostructural and microstructural architecture of the Karakoram fault: relationship between magmatism and strike-slip faulting. *Tectonics* 26, TC3017. <http://dx.doi.org/10.1029/2006TC001946>.
- Pokharel, R., Lind, J., Kanjarla, A.K., Lebensohn, R.A., Li, S.F., Kenesei, P., Suter, R.M., Rollett, A.D., 2014. Polycrystal plasticity: comparison between grain-scale observations of deformation and simulations. *Annu. Rev. Condens. Matter Phys.* 5, 317–346. <http://dx.doi.org/10.1146/annurev-conmatphys-031113-133846>.
- Prior, D.J., 1999. Problems in determining the misorientation axes, for small angular misorientations, using electron backscatter diffraction in the SEM. *J. Microsc.* 195, 217–225. <http://dx.doi.org/10.1046/j.1365-2818.1999.00572.x>.
- Prior, D.J., Boyle, A.P., Brenker, F., Cheadle, M.C., Day, A., Lopez, G., Peruzzo, L., Potts, G.J., Reddy, S., Spiess, R., Timms, N.E., Trimby, P., Wheeler, J., Zetterström, L., 1999. The application of electron backscatter diffraction and orientation contrast imaging in the SEM to textural problems in rocks. *Am. Mineral.* 84, 1741–1759. <http://dx.doi.org/10.2138/am-1999-11-1204>.
- Prior, D.J., Mariani, E., Wheeler, J., 2009. EBSD in the Earth Sciences: applications, common practice, and challenges. In: Schwartz, A., Kumar, M., Adams, B., Field, D. (Eds.), *Electron Backscatter Diffraction in Materials Science*. Springer, Boston, MA, pp. 345–360. http://dx.doi.org/10.1007/978-0-387-88136-2_26.
- Quintanilla-Terminel, A., Evans, B., 2016. Heterogeneity of inelastic strain during creep of Carrara marble: microscale strain measurement technique. *J. Geophys. Res. Solid Earth* 121, 5736–5760. <http://dx.doi.org/10.1002/2016JB012970>.
- Ralsler, S., Hobbs, B.E., Ord, A., 1991. Experimental deformation of a quartz mylonite. *J. Struct. Geol.* 13, 837–850. [http://dx.doi.org/10.1016/0191-8141\(91\)90008-7](http://dx.doi.org/10.1016/0191-8141(91)90008-7).
- Renner, J., Evans, B., Siddiqi, G., 2002. Dislocation creep of calcite. *J. Geophys. Res.* 107 (B12), 2364. <http://dx.doi.org/10.1029/2001JB001680>.
- Rowe, K.J., Rutter, E.H., 1990. Palaeostress estimation using calcite twinning: experimental calibration and application to nature. *J. Struct. Geol.* 12, 1–17. [http://dx.doi.org/10.1016/0191-8141\(90\)90044-Y](http://dx.doi.org/10.1016/0191-8141(90)90044-Y).
- Rutter, E.H., 1974. The influence of temperature, strain rate and interstitial water in the experimental deformation of calcite rocks. *Tectonophysics* 22, 311–334. [http://dx.doi.org/10.1016/0040-1951\(74\)90089-4](http://dx.doi.org/10.1016/0040-1951(74)90089-4).
- Rutter, E.H., 1995. Experimental study of the influence of stress, temperature and strain on the dynamic recrystallisation of Carrara marble. *J. Geophys. Res.* 100, 24651–24663. <http://dx.doi.org/10.1029/95JB02500>.
- Rutter, E.H., Faulkner, D.R., Brodie, K.H., Phillips, R.J., Searle, M.P., 2007. Rock deformation processes in the Karakoram fault zone, Ladakh, NW India. *J. Struct. Geol.* 29, 1315–1326. <http://dx.doi.org/10.1016/j.jsg.2007.05.001>.
- Schmid, E., 1928. Zn normal stress law. In: *Proceedings of the International Congress on Applied Mechanics*, Delft, 1924, pp. 342.
- Schmid, E., Boas, I.W., 1950. *Plasticity of Crystals*. Chapman and Hall, London, pp. 353.
- Scholz, C.H., 1988. The brittle-plastic transition and the depth of seismic faulting. *Geol. Rundsch.* 77, 319–328. <http://dx.doi.org/10.1007/BF01848693>.
- Skemer, P., Hansen, L.N., 2016. Inferring upper-mantle flow from seismic anisotropy: an experimental perspective. *Tectonophysics* 668–669, 1–14. <http://dx.doi.org/10.1016/j.tecto.2015.12.003>.
- Smith, S.A.F., Billi, A., Di Toro, G., Spiess, R., 2011. Principle slip zones in limestone: microstructural characterization and implications for the seismic cycle (Tre Monti Fault, central Apennines, Italy). *Pure Appl. Geophys.* 168, 2365–2393. <http://dx.doi.org/10.1007/s00024-011-0267-5>.
- Streule, M.J., Phillips, R.J., Searle, M.P., Waters, D.J., Horstwood, M.S.A., 2009. Evolution and chronology of the Pangong Metamorphic Complex adjacent to the Karakoram Fault, Ladakh: constraints from thermobarometry, metamorphic modeling and U Pb geochronology. *J. Geol. Soc.* 166, 919–932. <http://dx.doi.org/10.1144/0016-76492008-117>.
- Toy, V.G., Prior, D.J., Norris, R.J., 2008. Quartz fabrics in the Alpine Fault mylonites: influence of pre-existing preferred orientations on fabric development during progressive uplift. *J. Struct. Geol.* 30, 602–621. <http://dx.doi.org/10.1016/j.jsg.2008.01.001>.
- Turner, F.J., 1953. Nature and dynamic interpretation of deformation lamellae in calcite of three marbles. *Am. J. Sci.* 251, 276–298. <http://dx.doi.org/10.2475/ajs.251.4.276>.
- Van Buer, N.J., Jagoutz, O., Upadhyay, R., Guillong, M., 2015. Mid-crustal detachment beneath western Tibet exhumed where conjugate Karakoram and Longmu-Gozha Co faults intersect. *Earth Planet. Sci. Lett.* 413, 144–157. <http://dx.doi.org/10.1016/j.epsl.2014.12.053>.
- Verberne, B.A., Niemeijer, A.R., De Bresser, J.H.P., Spiers, C.J., 2015. Mechanical behavior and microstructure of simulated calcite fault gouge sheared at 20–600°C: implications for natural faults in limestones. *J. Geophys. Res. Solid Earth* 120, 8169–8196. <http://dx.doi.org/10.1002/2015JB012292>.
- Wallis, D., Hansen, L.N., Britton, T.B., Wilkinson, A.J., 2016a. Geometrically necessary dislocations in olivine obtained using high-angular resolution electron backscatter diffraction. *Ultramicroscopy* 168, 34–45. <http://dx.doi.org/10.1016/j.ultramic.2016.06.002>.
- Wallis, D., Hansen, L.N., Britton, T.B., Wilkinson, A.J., 2017. Dislocation interactions in olivine revealed by HR-EBSD. *J. Geophys. Res. Solid Earth.* <http://dx.doi.org/10.1002/2017JB014513>.
- Wallis, D., Phillips, R.J., Lloyd, G.E., 2013. Fault weakening across the frictional-viscous transition zone, Karakoram Fault Zone, NW Himalaya. *Tectonics* 32, 1227–1246. <http://dx.doi.org/10.1002/tect.20076>.
- Wallis, D., Phillips, R.J., Lloyd, G.E., 2014. Evolution of the eastern Karakoram metamorphic complex, Ladakh, NW India, and its relationship to magmatism and regional tectonics. *Tectonophysics* 626, 41–52. <http://dx.doi.org/10.1016/j.tecto.2014.03.023>.
- Wallis, D., Lloyd, G.E., Phillips, R.J., Parsons, A.J., Walshaw, R.D., 2015. Low effective fault strength due to frictional-viscous flow in phyllonites, Karakoram Fault Zone, NW India. *J. Struct. Geol.* 77, 45–61. <http://dx.doi.org/10.1016/j.jsg.2015.05.010>.
- Wallis, D., Carter, A., Phillips, R.J., Parsons, A.J., Searle, M.P., 2016b. Spatial variation in exhumation rates across Ladakh and the Karakoram: new apatite fission track data from the Eastern Karakoram, NW India. *Tectonics* 35. <http://dx.doi.org/10.1002/2015TC003943>.
- Wang, Z.-C., Bai, Q., Dresen, G., Wirth, R., Evans, B., 1996. High-temperature deformation of calcite single crystals. *J. Geophys. Res.* 101, 20377–20390. <http://dx.doi.org/10.1029/96JB01186>.
- Wenk, H.-R., Takeshita, T., Bechler, E., Erskine, B.G., Matthies, S., 1987. Pure shear and simple shear calcite textures. Comparison of experimental, theoretical and natural data. *J. Struct. Geol.* 9, 731–745. [http://dx.doi.org/10.1016/0191-8141\(87\)90156-8](http://dx.doi.org/10.1016/0191-8141(87)90156-8).
- Wheeler, J., Mariani, E., Piazzolo, S., Prior, D.J., Trimby, P., Drury, M.R., 2009. The weighted Burgers vector: a new quantity for constraining dislocation densities and types using electron backscatter diffraction on 2D sections through crystalline materials. *J. Microsc.* 233, 482–494. <http://dx.doi.org/10.1111/j.1365-2818.2009.03136.x>.